Internal Structure of Silver−Poly(amidoamine) Dendrimer Complexes and Nanocomposites

M. Francesca Ottaviani[†]

Institute of Chemical Sciences, University of Urbino, Piazza Rinascimento 6, 61029 Urbino, Italy

Regina Valluzzi

Tufts University, Department of Chemical and Biological Engineering, Medford, Massachusetts 02155

Lajos Balogh*

Center for Biologic Nanotechnology, University of Michigan, Ann Arbor, Michigan 48109-0533

Received March 21, 2001; Revised Manuscript Received January 29, 2002

ABSTRACT: Poly(amidoamine) PAMAM dendrimers of various generations (generation 2 to generation 6) with different surfaces (amine, Tris, and pivalate) were used as organic templates to form complexes and nanocomposites of silver. Starting from silver salts and PAMAM dendrimers, first a silver−dendrimer complex and then a nanocomposite were synthesized. To avoid chemical contamination, transformation of silver from Ag^+ to Ag^0 was achieved by irradiating the solution of silver complex with an excessive dose of X-rays. Intensity of the plasmon resonance at 400−420 nm was found to be the function of silver content, nanoparticle size, and architecture. Internal structural changes during this transformation from complexes into nanocomposites have been studied in the solution state by the electron paramagnetic resonance (EPR) technique. Copper(II) ions were used as a probe. Measurements were performed at various silver/dendrimer ratios and at various temperatures. We determined the structure of the copper(II) ions interacting with the [$(Ag^+)_n$−PAMAM] silver(I)−poly(amidoamine) dendrimer complexes and compared those to the structure of the respective Cu(II) complexes formed with {$(Ag^0)_n$−PAMAM} silver−dendrimer nanocomposites. In the presence of silver ions, the interior of the dendrimer was found to be partially positively charged and it repulsed copper ions, which were then confined to sites not occupied by silver ions. Transformation of Ag^+ into Ag^0 completely modified the Cu(II) interactions with the interior of the dendrimer in the direction of favoring the internalization of copper(II) ions in the dendrimer structure. In nanocomposites, Ag(0) atoms occupy the smaller outer cavities of the dendrimer interior forcing a portion of copper ions into the larger cavities. The conclusion above is also supported by high resolution energy-filtered TEM images of silver nanocomposites. The significance of various surface variations is also quantitatively described and discussed.

Introduction

Preparation of noble metal nanoclusters is very important in the development of optical materials, polymer conductors, catalyst carriers, and other applications. Formation of metallic silver particles from silver salts has been in the focus of interest since the discovery of photography. To achieve optimal performance, it is fundamental to control the size and polydispersity of the silver particles.

It has been shown that dendrimers are able to form complexes with a great variety of ions and compounds and act as excellent templates for nanoparticle fabrication.[1−6] Dendrimer templates offer usually better control over size, shape, and polydispersity than linear[7−9] polymers.

Dendrimer nanocomposites (DNCs) are organic/inorganic hybrid materials composed of nanosized particles displaying unique physical and chemical properties due to the atomic/molecular level dispersion of inorganic guest(s) and organic macromolecular hosts.[1] DNCs are made by reactive encapsulation, when dendrimers are used to preorganize small molecules or metal ions, followed by an in-situ immobilization of the resulting atomic or molecular domains of inorganic guests within or on their dendrimer host.[10] This method provides nearly uniform hybrid nanoparticles with an excellent control over size and size distribution.

Synthesis of silver dendrimer nanocomposites have been reported both by direct complexation[9,11] and by substitution of copper in the preformed {Cu(0)−PAMAM} copper nanocomposite.[12]

Nanocomposites of metallic silver and poly(amidoamine) PAMAM dendrimers {$Ag(0)_n$−PAMAM} are soft, nanosized spherical polymeric particles containing dispersed silver atoms and/or small silver clusters separated by the dendrimer wedges. They are stable and soluble in polar solvents, such as water and methanol. Primary structure of these nanocomposite particles (internal, external, mixed)[6] depends on the particular dendrimer (generation, surface, interior, etc.) and the conditions during fabrication.[1,6,10] Structurally, these materials are completely different from those when dendrimers are used as stabilizer for preformed crystalline silver colloids.[13,14]

Structure of these hybrid nanoparticles is in the focus of interest since the first report on DNC materials.[1] However, it is not a simple quest to gain reliable information on the formed structures in solution without changing the soft hybrid particles. TEM and HRTEM are often used to demonstrate the structure of a particular dendrimer nanocomposite, but sample prepa-

* Corresponding author. Telephone: (734) 615-0623. Fax: (734) 615-0621. E-mail: baloghl@med.umich.edu.
[†] Telephone: +39-0722-4164. Fax: +39-0722-2754. E-mail: ottaviani@uniurb.it.

10.1021/ma010492f CCC: $22.00
Published on Web 05/21/2002

ration procedures used in these techniques make it impossible to obtain reliable overall information about the hybrid DNC structure existing *in solution*. Small-angle scattering is the method of choice to determine average particle sizes,[15] but this technique grants no information about the internal structure of the metal−dendrimer complexes and the nature of the connections between host and guest.

A typical procedure for synthesizing internal type silver−dendrimer nanocomposites from silver complexes of Tris-terminated PAMAM dendrimers by photolysis has previously been reported.[6] It was observed that the size of dendrimers usually is not altered by the metal ion complexation.[16] In preliminary experiments, solutions of silver−PAMAM complexes proved to be quite insensitive to light: 1 day exposure to daylight resulted in only approximately 50% conversion based on the increase of intensity of the 420 nm plasmon peak in the visible spectra. Long-term photolysis of the complexed silver ions generated silver(0) nanocomposites, in which the homogeneous distribution of silver within the dendrimer-defined nanodomains was retained upon transformation. This was also supported by the UV−visible spectra displaying only one major symmetric plasmon peak at 420 nm.[16] On the basis of TEM images, it was also concluded that silver atoms did not migrate considerably in the organic template within the time scale of the investigation.[9] According to the featureless and very poor XRD spectra of nanocomposites, these internalized metallic domains are small, are amorphous, and have a very low degree of crystallinity.

Our goal was to determine the structure of the silver ion complexes and nanocomposites and identify the structural differences between silver complexes and nanocomposites. Thus, we studied the ligand structure of $[(Ag^+)_n-PAMAM]$ silver(I) poly(amidoamine) dendrimer complexes and the respective $\{(Ag^0)_n-PAMAM\}$ silver(0) dendrimer nanocomposites of various PAMAM dendrimers by EPR and energy-filtering TEM.

In general, location of the Ag(0) domains depends on the metal/dendrimer ratio, the structure of the template, the kinetics of the immobilizing reaction, and the fabrication procedure. It has originally been assumed that silver ions have randomly filled positions in PAMAM complexes and these positions are determined by the availability of electron donor ligands (tertiary nitrogen branching sites). When silver-DNCs formed in photolysis (i.e., in a process which does not require the diffusion of an other reactant to the silver ions), metal atoms should originally form and appear at the same location where they were bound to the dendrimer structure even though they may undergo redistribution in the polymeric phase of the hybrid nanoparticles.

Electron paramagnetic resonance (EPR) technique was successfully applied before[19,20] to gain insight into the detailed structure of copper(II) complexes of the amine and methylester terminated PAMAM dendrimers. Selection of copper(II) ions as reporter ions is well justified, since their chemistry, spectral properties and ligand character have extensively been investigated.[17,21] Details of Cu(II) complexation with PAMAM dendrimers have also been examined in details by UV−visible spectroscopy,[2,3,22] by small-angle neutron and X-ray scattering,[16] and by the combination of ultrafiltration and ion-selective concentration measurements[18] both in aqueous and methanol solution.

Scheme 1. General Experimental Scheme of This Study Using a Generalized Generation 2 Dendrimer[a]

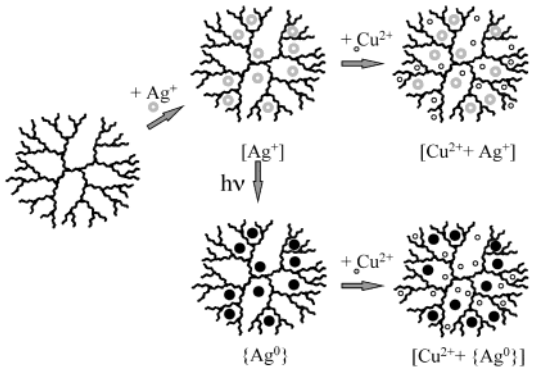

[a] Silver ions (large, empty gray circles), silver atoms (large black full spots), and copper(II) ions (small black circles) are shown.

EPR spectra were detected by adding known amount of copper(II) ions to the preformed silver−dendrimer complexes in comparable concentrations. The same procedure was applied to the solutions of silver nanocomposites made by the X-ray irradiation from the aliquot parts of the silver−PAMAM complex solutions (Scheme 1). Computer-aided analysis of the EPR spectra provided information on the formation of copper complexes in various internal or external locations of the dendrimers, as well as the structure of the complexes and nanocomposites as a function of the size and surface of the dendrimers, temperature, silver content, etc.

Energy-filtering TEM was also utilized to confirm and illustrate the structure of the silver nanocomposite particles. Energy-filtering TEM uses the fact that electrons can interact with a sample in a number of ways, including elastic (forward scattering, energy is unchanged) and inelastic scattering. Inelastic scattering results from interactions with the sample where electrons experience energy loss. Electrons can interact inelastically with a sample plasmon, or with atoms in the sample generating an energy loss spectrum corresponding with different aspects of the sample material experienced by the electrons. Element specific energy loss may then be quantitized and can be used to map elements and generate element specific contrast. Energy loss due to plasmon interactions can also be used to provide enhanced contrast in polymers.

Experimental Section

Materials. In this work, poly(amidoamine) dendrimers were used. Amine terminated ethylenediamine core PAMAM dendrimers were purchased from Dendritech, Midland, MI, and were used without further purification. Technical grade chemicals were used with >85% generational dendritic purity.

Tris- and pivalate-terminated PAMAM dendrimers were prepared according to the literature.[5]

These combinations of terminal groups offered cationic and strong electron-donor $-NH_2$ and polar and weak proton donor $-NH-C(CH_2OH)_3$ groups as well as hydrophobic $-NH-CO-C(CH_3)_3$ terminal groups with a comparable number of nitrogen ligands and dendrimer template sizes (see Table 1).

High purity $AgNO_3$ and methanol were purchased from Aldrich and were used without further purification. Cupric nitrate was purchased from Sigma and used as received.

Preparation of Silver−Dendrimer Nanocomposites.[26] To reflect the contribution of architectural differences among various dendrimer templates, both the total concentration of N ligands (approximately 0.1 M) and the concentration of silver ions (6.26×10^{-3} M) were kept constant. This silver concentra-

Table 1. Main Properties of PAMAM Dendrimers Used (Significant for This Study)

shorthand	terminal groups	theoretical no. of subsurface tertiary N	possible position of ion bonding
E4.Tris	64 $-C(CH_2OH)_3$	62	interior
E5.NH_2	128 $-NH_2$	126	interior + exterior
E5.P	128 $-C(CH_3)_3$	126	interior

Table 2. Data of Silver−Dendrimer Complexes and Nanocomposites[a]

dendrimer	M_n	$-NH_2$	$-N=$	tot. no. of N	[tot. N], mol/L	[D], mol/L	Ag/D
E2.A	3256	16	14	32	9.96E−2	3.32E−3	3.77
E3.A	6909	32	30	62	1.01E−1	1.63E−3	7.66
E4.A	14 215	64	62	126	1.06E−1	8.37E−4	14.96
E5.A	28 826	128	126	254	8.93E−2	3.52E−4	35.62
E6.A	58 048	256	254	510	1.04E−1	2.03E−4	61.75
E4.T	18 124	0	62	62	1.05E−1	1.69E−3	7.41
E3.P	9597	0	30	30	1.01E−1	3.37E−3	3.71
E5.P	50 613	0	126	126	9.94E−2	7.89E−4	15.87

[a] Dendrimer−NH−Z, where Z = A denotes primary amine termini, i.e., dendrimer-NH_2 end group structure; T = Tris, i.e., dendrimer−NH−$C(CH_3)_3$; and Z = P, where P = pivalate, i.e., dendrimer−NH−$COC(CH_3)_3$, termini.

tion was estimated to be a 50% capacity of the dendrimer total silver binding ability, allowing measurable amount of copper ions to bind. (Relative ratio of reporting ions was between 1.5 and 24.6 Cu^{2+}/dendrimer molar ratio from the generation 2 to the generation 6 dendrimer complexes and nanocomposites.)

Complexation. For complexation experiments, silver nitrate was selected because of its good solubility both in water and in methanol. To ensure identical silver concentration 0.1064 g $AgNO_3$ was dissolved in 50 mL of DI water and 5 mL aliquots were used. Thus, a typical procedure was, as follows: 5 mL of silver nitrate stock solution (10.64 mg $AgNO_3$) was added dropwise with stirring to the weighed amount of PAMAM dendrimer stock solution (20% w/w in methanol). The volumetric flask was filled up to 10.00 mL with methanol resulting in a 1:1 = water/MeOH solution of sample containing 0.1 M nitrogen ligands and 5.32 mg of silver ion ($[Ag^+] = 6.263 \times 10^{-3}$ M) for the investigated solutions.

The metal ion/dendrimer ratio is predetermined by the ratio of metal ion moles per dendrimer moles due to the uniformity of dendrimers and the isotropic nature of the diffusion. Accordingly, individual dendrimers will form complexes with an equal and well-defined number of metal atoms per dendrimer molecule which are expressed as average numbers (Table 2).

Photolysis. To ensure complete conversion of silver ions, X-ray irradiation was used with a dose rate of 1.5 Gy/min. The vials containing silver−dendrimer complex solutions were submerged in water. The vials were irradiated from the side for appropriate buildup of dose. The applied doses were 2 × 1000 rad to make sure that the photolysis is complete.

Exposure of the complex solutions to visible light over an extended time yielded yellow to light brown silver nanocomposite solutions, which were stable even at 10% w/w nanocomposite solutions. DNC solutions were stored in Parafilm-sealed volumetric flasks under nitrogen in the dark at room temperature.

Preparation of the Samples for EPR Analysis. Stock solutions of cupric nitrate were prepared in dry methanol and added to the dendrimer solutions to obtain final concentrations of 0.01 and 0.005 M in Cu^{2+} and 0.2 M in dendrimer external surface groups (for simplicity and for a better comparison with previous works,[19,20] the dendrimer concentration in the EPR analysis was calculated in external surface groups). About 100 μL of freshly prepared solutions were inserted in 2 mm glass tubes, sealed, and immediately processed by EPR. Indeed, aging of the solutions did not change the results for at least 1 month.

Energy Filtering TEM. TEM samples were prepared as reported previously.[6] In some of the images, contrast appears inverted because we were using the energy filter to create an image using inelastically scattered electrons. Dendrimers are visible as white spots in these images (and can be virtually invisible in normal TEM). The resolution is lower in the inelastic images because (A) a lower proportion of the electrons hitting the sample was used to form the image resulting in increased speckling and (B) a fairly wide slice of the inelastic loss spectrum (i.e., electrons with a variety of energies) was used to focus and form an image, which sometimes results in chromatic aberration, etc. By selecting a "slice" of inelastically scattered electrons, we can distinguish the polymeric dendrimers from the polymeric film substrate used in sample preparation, because the two substances have different inelastic interactions with electrons (even though their elastic interactions are virtually identical). Inelastic interactions are very sensitive to the electronic structure of the sample.

The "normal" images are elastic brightfield ones—the inelastic electrons have been filtered out to maximize crispness and contrast from the elastic electrons. In an unfiltered TEM image, a high magnification image is created using electromagnetic lenses after the electron beam interacts with the sample. Inelastic interactions between the electrons and the sample result in a spectrum of electron energies in the beam after it interacts with the specimen, resulting in increased chromatic aberration which limits both contrast and resolution. In an elastically filtered image, the aberration and background from nonelastic interactions with the sample is removed, resulting in high contrast images even at high voltages.

Techniques. The starting materials and the obtained products were carefully characterized by different analytical techniques. UV−visible spectra were obtained on a Perkin-Elmer Lambda 20 spectrophotometer at room temperature between 200 and 1100 nm in a Suprasil 300 quartz cell (L = 1 mm). ^1H and ^{13}C NMR measurements were carried out on a Bruker 500 multinuclear spectrometer equipped with a temperature controller. Size exclusion chromatography was performed on three TSK gel columns (4000, 3000, and 2000) using a Waters 510 pump with a Wyatt Technology Dawn DSP−F MALLS and Wyatt Technology 903 interferometric refractometer and a Waters 510 pump with a Waters 410 differential refractometer, respectively.

An AECL Theratron 80 high intensity cobalt-60 source was used to irradiate the silver complex solutions.

Energy-filtering TEM images were taken at Leo Electron Microscopes in Oberkochen, Germany, using Formvar coated carbon grids after appropriate dilution. A LEO 922 with a high-resolution pole piece and an Omega energy filter was used to obtain energy filtered images of the dendrimers at 200 kV. Images were captured using a slow scan CCD camera. Grids were screened prior to analysis in Germany at the University of Massachusetts Amherst using a JEOL 2000 Mark II with a high-resolution pole piece operated at 200 kV and images were collected on "Kodak electron image plates" EM film. The grids used for HRTEM were carbon support film 400 mesh copper grids. The carbon films were rendered hydrophilic by plasma cleaning. γ-Irradiated silver nanocomposites were imaged. A glovebox with a dry nitrogen atmosphere was used to prevent change of oxidation state of the metals within the dendrimer nanocomposites during sample preparation.

EPR spectra were recorded by means of a EMX-Bruker instrument interfaced to a PC computer with the Bruker software for spectra recording and handling. The temperature was controlled by means of a Bruker ER4131VT temperature controller. Magnetic parameters were measured referring to 1,1-diphenyl-2-picryl-hydrazyl (DPPH) standard (g = 2.0036) and evaluated by suitable computer programs for spectral computation. Low-temperature spectra, typical of Cu(II) in a glasslike environment, were computed by means of the CU23GP program, kindly provided by Prof. Romanelli, University of Florence, Florence, Italy. Accuracy in determining the magnetic and mobility parameters, as well as the relative percent-

ages of the spectral components, was 5%, as obtained from the fitting between the experimental and the computed signals.

Results and Discussion

Dendrimers of various generations (generation 2 to generation 6) with different surfaces (primary amine, tris(hydroxymethylamino)methane, and pivalate) were used as templates and as organic components of the nanocomposites. Complexation of metal ions depends on the metal/dendrimer ratio and the composition, generation, and structure of the PAMAM dendrimers, but it does not depend on the dendrimer concentration itself.[23,9,11] In our experiments, both the overall concentration of nitrogen ligands as well as the silver ion concentration were kept constant. Variation in the silver/PAMAM relative molar ratio therefore is expected to be the result of the variations in template architecture and generation.

The concentration of the dendrimers was kept sufficiently low (Table 2) not to favor intermolecular bonding between the templates, since aggregation of templates may occur in solution, and it has also been demonstrated that Ag−N coordination bonds can be reliably used for the construction of supramolecular networks.[23] In the case of silver−PAMAM complexes, these networks could form within the dendrimers and between the complex containing macromolecules when primary amine surface groups are present that can act as ligands (as opposed to *tert*-butyl and Tris termini).

Dendrimer−silver complexes were transformed into nanocomposites by irradiating the $[(Ag^{+})_n-PAMAM]$ aqueous solutions with an excessive dose of gamma-rays to avoid the introduction of further chemicals. Scheme 1 delineates the general procedure followed.

Since silver does not have a measurable signal in EPR, copper(II) ions were used as a probe. On the basis of general stability constants, copper(II) complexation with small molecules is preferred to silver(I) with otherwise identical nitrogen ligands.[21] Due to the equilibrium nature of the complexation process, a redistribution of complexing sites is expected to take place when both Cu(II) and Ag(I) ions are present. In other words, Cu^{2+} ions will compete with Ag^{+} ions in the mixed complexes and they will occupy the space available in the dendrimer structure.

Cu(II) ions will not disturb the structure of the preformed silver(0) DNC, because silver is a less electronegative metal, and it has been shown that silver substitutes copper in its compounds[21] and in preformed {Cu(0)−PAMAM} copper nanocomposites.[14] However, Cu(II) complexation will be hindered near ligand sites preoccupied by the silver atoms in the hybrid nanocomposite particles. As a consequence, ligand structure of Cu(II) complexes of nanocomposites will provide indirect but useful structural information regarding the positioning of silver ions and metallic silver domains in the host dendrimers. In our study, the structures of Cu(II) complexes were detected and analyzed for information regarding the silver components.

Intensity of the silver plasmon resonance in the DNC solutions was found to be a function of nanoparticle size and architecture: it was observed to be increasing for increasing generations of amine-terminated PAMAMs (Figure 1). Increasing intensity suggests increasing nanoparticle size or increased concentration.[25] As the overall silver concentration (and silver/nitrogen ratio) was kept constant throughout the nanoparticle fabrication process, the molar concentration of the templates was observed to be decreasing with increasing dendrimer generations and the number of silver ions per macromolecule was observed to be increasing. (Every generation roughly doubles the molecular mass of a PAMAM.) It is demonstrated in both Figures 1 and 2 that the intensity of the silver plasmon peaks clearly increases with increasing generations until the overall diameter of the DNC reaches about 4 nm. The low intensity peaks observed for $\{(Ag^0)_{3.71}-PAMAM\_E3.P\}$ and $\{(Ag^0)_{7.41}-PAMAM\_E4.T\}$ nanocomposites can be explained with the formation of internal nanocomposites that contain smaller metal domains. Tris- and pivalate-terminated dendrimers can form internal silver complexes only as their terminal groups do not interact.

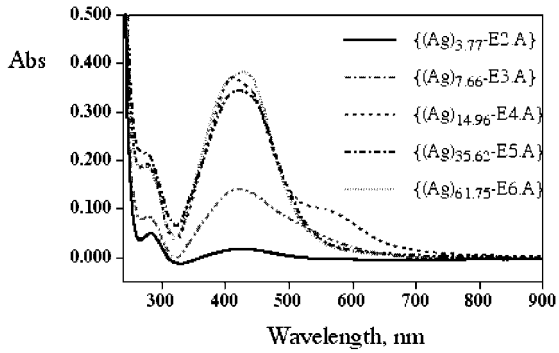

Figure 1. Comparison of UV−visible spectra of $\{(Ag^0)_n-PAMAM\_Em.A\}$ nanocomposites after X-ray treatment. E = ethylenediamine core, n = average number of complexed silver ions per dendrimer (See Table 2), m = generation number, and A = amine-terminated.

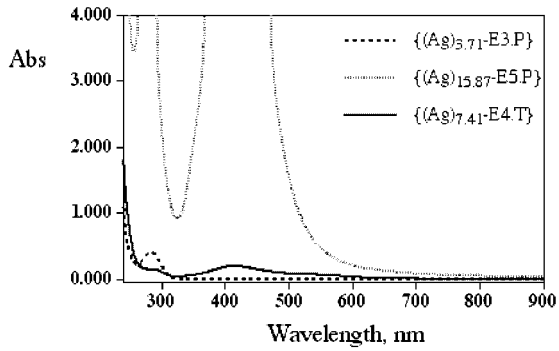

Figure 2. Comparison of UV−visible spectra of $\{(Ag^0)_{3.71}-E3.P\}$, $\{(Ag^0)_{15.87}-E5.P\}$, and $\{(Ag^0)_{7.41}-E4.T\}$ nanocomposites after X-ray treatment. E = ethylenediamine core, n = average number of silver atoms per dendrimer, m = generation, and P = pivalate-terminated and T = Tris-terminated polymers.

$\{(Ag^0)_{15.87}-PAMAM\_E5.P\}$ displayed a surprisingly intense plasmon resonance (Figure 2). One can speculate that in the case of a dense dendrimer surface structure, such as for PAMAM_E5.P complexes and nanocomposites may form only in the peripheral region. A more detailed investigation is in order to explain this observation.

EPR Analysis of the Cu(II) Complexes of the Silver−Dendrimer Complexes $[(Cu^{2+})_i(Ag^{+})_n-Em.A]$, $[(Cu^{2+})_j(Ag^{+})_n-Em.P]$, and $[(Cu^{2+})_i(Ag^{+})_n-PAMAM\_Em.T]$. EPR samples have been prepared with Cu(II) at 0.01 and 0.005 M present in the samples. EPR spectra were recorded at 160, 298, and 358 K. Analysis of both room temperature and low-temperature spectra was carried out by means of suitable computer programs. The spectral computation allowed us to

extract the magnetic parameters, namely the components of the **g** tensor for the Zeeman coupling between the electron spin and the magnetic field and the components of the **A** tensor for the coupling between the electron spin and the nuclear spin. The increase in **A** components with the correspondent decrease in the **g** components of powder spectra arises from a variation in Cu(II) coordination, such as substitution of oxygen ligands with nitrogen ligands, and a variation in the complex structure. By comparison of the magnetic parameters with those found in the literature for several Cu(II) complexes, the coordinating groups and the structure of the complexes are proposed. All the spectra shown in the present study are typical of Cu^{2+} complexes with an elongated octahedral structure (square planar, with $d_{x^2-y^2}$ ground level), and an almost axial symmetry ($g_{zz} > g_{xx} \approx g_{yy}$). Also, the line widths are included as input data in the calculation. An increase in line width is often attributable to inhomogeneous sources and spin−spin interactions. The room-temperature spectra were analyzed by means of the program of Schneider and Freed,[24] which not only allows us to confirm the magnetic components evaluated from the analysis of the spectra at low temperature and, therefore, the proposed coordination and structure of the complexes but also let us evaluate the correlation time for the reorientational mobility, τ_c. "Slow motion" conditions correspond to $1 \times 10^{-9}\text{s} < \tau_c < 5 \times 10^{-7}$ s and led to a partial resolution of the anisotropy of the magnetic components. It was possible to evaluate the "not rigid" components, $A_{||}'$, $g_{||}'$ and $g_{\perp}'$ (usually $A_{\perp}'$ is too small to be evaluated). "Fast mobility" and "rigid mobility" are of course at the two outer extremes ($\tau_c < 1 \times 10^{-9}$ s and $\tau_c > 5 \times 10^{-7}$ s, respectively).

The best fit between the experimental and the computed spectra was obtained by using several input parameters, with an accuracy of about 5%. Input parameters above or below the accuracy limit changed the computed line shape and decreased the accuracy in the fitting. Of course, we cannot exclude that different sets of parameters might produce a better fitting with the experimental signals, but we are confident with the obtained computations for the following reasons: (a) each parameter usually produces a different modification in the computed line shape; (b) the selected set of parameters was obtained after several attempts of computation, by a trial and error procedure, changing each parameters and controlling the fitting; (c) the physical meaning of the parameters also limit the possibility of changing the selection; (d) the fitting of series of spectra of the same system, but changing the experimental conditions (such as temperature or concentration), was obtained by means of the same set of parameters, only changing the parameter which was expected to be modified by the physical modifications of the system.

The increase in Cu(II) concentration from 0.005 to 0.01 M (results not shown) led to (a) a small broadening of the EPR lines, attributable to inhomogeneous line broadening, (b) an increase in the component belonging to noninteracting Cu(II) ("external component", indicated as Comp. A), and (c) a decrease in the signal-to-noise ratio.

However, the absence of spin−spin effects indicates that the higher concentration does not produce occupation of close sites in the dendrimer structure by Cu(II) complexing surface groups. Furthermore, since the spectra are mainly constituted by different components corresponding to different Cu(II)−dendrimer coordinations, the distribution of Cu(II) in different dendrimer environments is not modified by the higher Cu(II) concentration. We henceforth describe and discuss the spectra obtained from 0.005 M solutions.

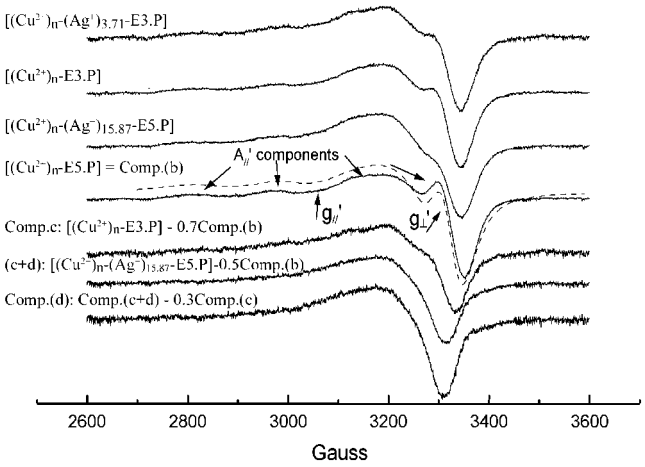

Figure 3. EPR experimental spectra (full lines) at 298 K of the pivalate-terminated dendrimer samples in the absence ([$(Cu^{2+})_n$−E3.P] and [$(Cu^{2-})_n$−E5.P]) of silver ions and in the presence of silver ions ([$(Cu^{2+})_n(Ag^{+})_{15.87}$−E5.P] and [$(Cu^{2+})_n$-$(Ag^{+})_{3.71}$−E3.P]). The figure also shows the various signals extracted using a subtraction procedure described in the text. In the figure, the $A_{||}$, $g_{||}'$ and $g_{\perp}'$ parameters are indicated in the [$(Cu^{2+})_n$−E5.P] spectrum for which the calculated spectrum (dashed line) is also shown.

Surprisingly, the spectra underwent really small changes between 298 and 358 K (results are not shown). The spectra at 298 K still show conditions of restricted mobility for Cu(II) interacting with the dendrimer structure. Figure 3 shows the EPR spectra at 298 K of the pivalate-terminated dendrimers in the absence [$(Cu^{2+})_n$−PAMAM_E3.P] and [$(Cu^{2+})_n$−PAMAM_E5.P] and in the presence [$(Cu^{2+})_n(Ag^{+})_{3.71}$−PAMAM_E3.P] and [$(Cu^{2+})_n(Ag^{+})_{15.87}$−PAMAM_E5.P] of complexed silver ions. In the figure, the $A_{||}'$, $g_{||}'$ and $g_{\perp}'$ components, characteristic of slow mobility, are indicated. Similar mobility conditions are usually found at about 200 K for Cu(II) complexes in solution with "small" ligands. *Such mobility quenching is expected on the basis of Cu(II) trapped in the dendrimer structure and coordinated to surface sites at the dendrimer branches.* Similar results have been previously found for Cu(II) complexed by PAMAM dendrimers at high generation and high pH.[20] The increase in temperature from 298 to 358 K led to a small increase in mobility: the spectral line shape remained almost unchanged in this range of temperature. This result may be interpreted on the basis of the *increased rigidity of the dendrimer structure due to the presence of the silver atoms*. We henceforth describe and discuss the spectra obtained at 298 K.

The dashed line in Figure 3 is the spectrum (Comp. (b)) computed by means of the program of Schneider and Freed.[24] The magnetic parameters used for computation were the ones used for the spectra at low temperature (Comp. (B), see below). The mobility parameter from computation—namely, the correlation time for the reorientational mobility, τ_c—is indicative of slow motion, that is, $\tau_c = 2 \times 10^{-9}$ s. This spectrum provides a good fitting of the experimental signal from the [$(Cu^{2+})_n$-$(Ag^{+})_{15.87}$−PAMAM_E5.P] and [$(Cu^{2+})_n$−PAMAM_E5.P] in methanol. Comparing the spectrum of [$(Cu^{2+})_n$−E5.P]

with the other EPR signals, a different line broadening is evident for the different samples. Besides, a simple increase in line width in the spectral computation cannot reproduce the line shape variation of [$(Cu^{2+})_n$−E5.P] between [$(Cu^{2+})_n$−E5.P] and the other samples. A subtraction procedure allows the extraction of further signals (bottom spectra). The subtraction of 70% of Comp. (b) from the spectrum of [$(Cu^{2+})_n$−E3.P] produces a second component, termed Comp. (c), still in slow motion, in which the variation of the magnetic parameters, in correspondence with the low-temperature Comp. (C) (see below), is indicative of the change in Cu(II) coordination toward a substitution of nitrogen ligands with oxygen ligands. The subtraction of 50% of Comp. (b) from the spectrum of [$(Cu^{2+})_n(Ag^+)_{3.71}$−PAMAM_E3.P] produces the same Comp. (c) (result not shown). On the contrary, subtraction of 50% of Comp. (b), i.e., [$(Cu^{2+})_n$−E5.P], from the spectrum of [$(Cu^{2+})_n(Ag^+)_{15.87}$−E5.P] leads to a different signal. The hypothesis that this signal still contains the Comp. (c) is true: subtraction of 30% of Comp. (c) extracts a third component, termed Comp. (d), which is broad and unstructured, likely due to Cu^{2+} not interacting with the dendrimer surface, but only with solvent molecules. Summarizing these results we get the following:

spectrum [$(Cu^{2+})_n(Ag^+)_{3.71}$−PAMAM_E3.P] =
50% Comp. (b) + 50% Comp. (c)

spectrum [$(Cu^{2+})_n$−PAMAM_E3.P] =
70% Comp. (b) + 30% Comp. (c)

spectrum [$(Cu^{2+})_n(Ag^+)_{15.87}$−PAMAM_E5.P] =
50% Comp. (b) + 30% Comp. (c) + 20% Comp. (d)

spectrum [$(Cu^{2+})_n$−PAMAM_E5.P] =
100% Comp. (b)

Of course, we trust these results only to the extent to which they correspond to the results acquired at low temperature. Figure 4a shows the EPR spectra of Cu^{2+} ions complexed in pivalate-terminated dendrimers (generations 3 and 5) at 160 K in the absence and in the presence of Ag^+. The computed spectra (dashed lines) were obtained by means of the following procedure.

(a) First, a subtraction−addition procedure was performed to extract the different components, using (and consequently verifying) the component percentages found at room temperature. Small variations in the percentages were found, which are expected for the different accuracy in the calculation (for instance, Comp. (c) and Comp. (d) are partially superimposable, whereas the correspondent components at low temperature are well distinguished);

(b) Then each component was computed: Figure 4b shows the three components, termed Comp. B, Comp. C, and Comp. D, related to the corresponding components at room temperature, and their computation; the magnetic parameters used for computation are also indicated in the figure. From the comparison of the magnetic parameters to those found for Cu(II) complexes with PAMAM dendrimers,[19,20] and in line with these previous results, *we attribute Comp. B* (*and Comp. (b)* at room temperature) *to Cu(II) interacting with three to four amino groups at the dendrimer surface (substituting methanol molecules), that is, a Cu[N_3O] or Cu[N_4] complex.* Again in line with previous results on Cu(II)−dendrimer complexes,[19,20] *Comp. C is attributed to Cu(II) interacting with two nitrogen ligands and two oxygen ligands, that is, a Cu[N_2O_2] complex. Comp. D arose from a Cu(II) solution which separates at low temperature* forming an undissociated salt (probably internal to the dendrimer, since this component is present at room temperature as Cu^{2+} solution = Comp. (d)). Previous studies with PAMAM dendrimers[19,20] also showed the formation of Comp. D upon freezing of the samples.

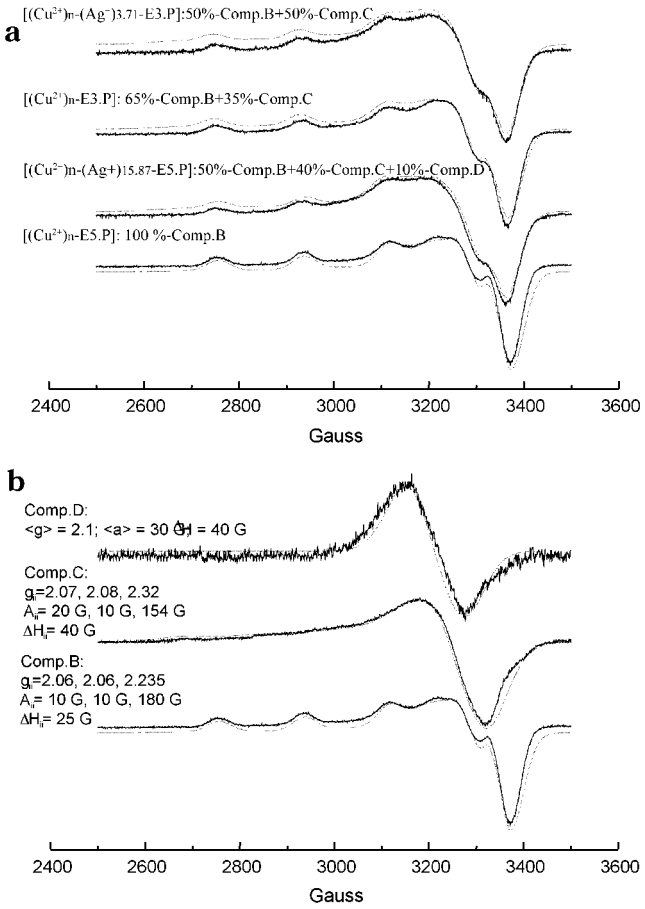

Figure 4. (a) EPR experimental spectra (full lines) of [$(Cu^{2+})_n$−E3.P] and [$(Cu^{2+})_n$−E5.P] complexes at 160 K. The computed spectra are shown as dashed lines. (b) Three EPR components (full lines) extracted from the experimental spectra in part a by means of the subtraction-addition procedure described in the text. The computed signals are also shown as dashed lines together with the magnetic parameters used for computation.

(c) Finally, the computed components were combined in the same ratios as they were extracted previously to simulate the experimental line shape reported in Figure 4. Percentages of the components which produced the best fit of the experimental with the computed spectra are also indicated in Figure 4.

Summarizing, spectral analysis of Cu(II) complexes of the PAMAM_E3.P and PAMAM_E5.P dendrimers and the [$(Ag^+)_{3.77}$−PAMAM_E3.P] and [$(Ag^+)_{15.87}$−PAMAM_E5.P] pivalate dendrimer complexes resulted in the following conclusions.

1. The coordinations of the dendrimers are similar as found earlier with PAMAM dendrimers.[19,20]

2. Cu(II) in E5.P mainly coordinates to the amino groups internal to the dendrimer structure, since the mobility of the complexes remains slow even at high temperature.

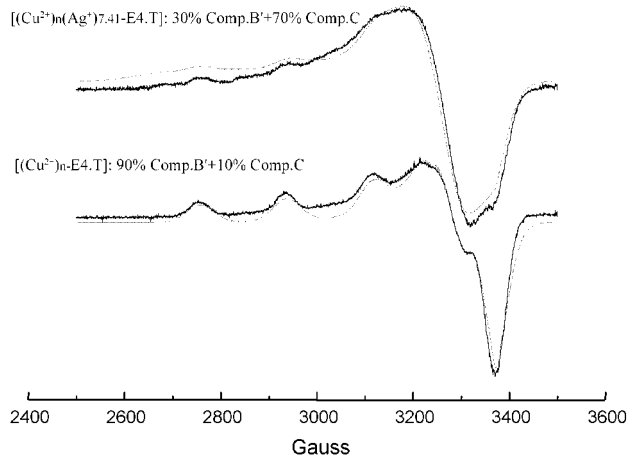

Figure 5. EPR experimental spectra (full lines) in the absence $[(Cu^{2+})_n-E4.T]$ and in the presence $[(Cu^{2+})_n(Ag^+)_{7.41}-E4.T]$ of silver ions at 160 K. The computed signals are also reported (dashed lines).

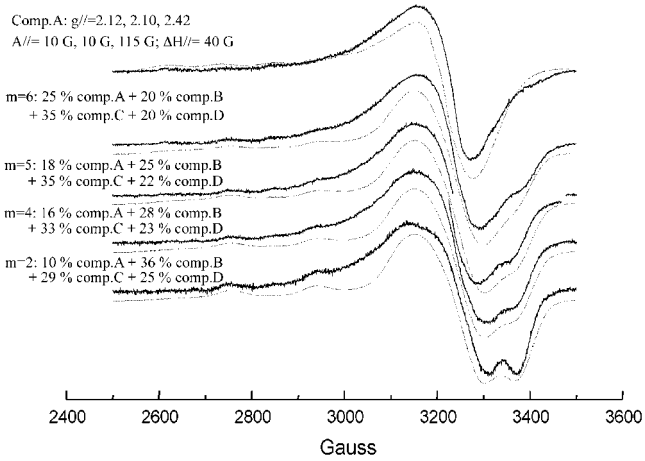

Figure 6. EPR experimental spectra (full lines) recorded from $[(Cu^{2+})_k\{(Ag^0)_l-Em.A\}]$ Cu^{2+} complexes of silver(0) nanocomposites of various generations of amine-terminated dendrimers at 160 K. The dashed lines are the computed spectra.

3. Decrease in generation (from E5.P to E3.P) leads to the appearance of a further component, which shows a decrease in the number of coordinating nitrogen ligands. Most likely, the more open structure of the dendrimer facilitates the entering of solvent molecules which takes the nitrogen ligands farther from each other and from the Cu(II) ions. However, the complex still shows slow mobility at room temperature, indicating the internalization of Cu(II) in the dendrimer structure.

4. The presence of silver ions in the dendrimer decreases the number of available nitrogen ligands thus increases the average distance between the available uncomplexed nitrogens within the same polymer molecule. This effect appears as the decrease of the $Cu[N_3O]$ chromophores in favor of $Cu[N_2O_2]$, i.e., the main effect of silver ions is hindering Cu(II)−N coordination.

5. Furthermore, a third component appears in the Cu(II) complex of $[(Ag^+)_{15.87}-PAMAM\_E5.P]$, that is, excess Cu^{2+} in uncomplexed Cu(II) solution which separates as $CuCl_2$ salt at low temperature. The occurrence of this behavior may be attributed to the entrapment of Cu(II) ions inside the dendrimer structure in regions mainly occupied by silver, which in turn restricts the space available to the paramagnetic ions.

The change of the $-C(CH_3)_3$ terminal pivalate groups to $-C(CH_2OH)_3$ Tris groups in PAMAM_E4.T and $[(Ag^+)_{7.41}-E4.T]$ affects the complexing behavior of Cu(II). The room-temperature spectra (not reported) show a lower mobility of the Cu−dendrimer complex. This means that *Tris terminal groups provide a stronger constraint of the dendrimer structure than pivalate does in the region in which the complex forms.*

The spectra at 160 K for $[(Cu^{2+})_n-E4.T]$ with and without Ag^+ are reported in Figure 5. The computation indicated superposition of Comp. B′, (only differing from Comp. B for an increase in line width,) and Comp. C. The increase in line width, in parallel with the room-temperature results, may arise from the increased constraint of the dendrimer structure which forces the Cu ions to stay closer to each other. It is noteworthy that the formation of silver ion nanoclusters provokes a marked increase in Comp. C at the expenses of Comp. B′. *The internal silver ions modify the dendrimer structure and prevent coordination of Cu(II) with more than two nitrogen sites, resulting in increased coordination with solvent molecules.*

A more intricate situation is found for $[(Cu^{2+})_n(Ag^+)_m-PAMAM\_En.A]$, for the silver complexes of the amino-terminated dendrimers. The room temperature spectra (not reported) indicated an increased mobility of the copper complexes. Figure 6 shows the EPR spectra recorded from these dendrimer complexes at low temperature. The dashed lines in Figure 6 are the computed signals. The procedure of computation is the same as described above: first of all a subtraction procedure was carried out, followed by computation of the extracted components; finally, the computed components were composed at the determined ratios to provide the fitting of the experimental signals.

For the sake of simplicity, EPR spectra of the [Cu(II)−PAMAM] dendrimer complexes are not shown. The line shape in these spectra is almost the same as found in water,[23] and it is comparable to the spectra shown for pivalate and Tris-terminated compounds, that is, mainly composed from Comp. b and Comp. B at room and low temperature, respectively.

The analysis of the EPR spectra of Cu(II) complexes with $[(Ag^+)_m-PAMAM\_En.A]$ indicated the presence of at least four well-distinguishable components at low temperature. A further component was found in the spectra, termed Comp. A. Comp. A and its computed signal are shown in Figure 6 (top spectrum). The magnetic parameters obtained from computation and the fast mobility at room temperature suggests that this component arises from *solvated Cu(II) ions that are not in interaction with the dendrimer surface, but are affected by the surface in the sense that no salt separation occurs upon freezing of the solution for this fraction of Cu(II) ions.* This signal was already found for Cu(II) in PAMAM dendrimer solutions,[19,20] mainly at low pH and low generation, since protonation of the amino groups prevents Cu(II) coordination. It is noteworthy that in the present case the noninteracting component A increases at the expense of Cu(II)−dendrimer components (mainly B) with the increase in generation. This suggests that binding of *Ag^+ ions in the highly packed large dendrimers is preferred to Cu(II) ions, which is reflected in the increasing amount of the Cu−solvent complex. This phenomenon also produces a small increase in Comp. C (which indicates Cu(II) interacting with two amino groups and two external solvent molecules).*

Finally, Comp. D is present to a good extent at low temperature, whereas it is absent at room temperature.

In this case, Comp. D arises from the Cu(II) salt, which separates from the external solution upon freezing. The smaller fraction of Comp. D at high generation with respect to low generation is expected since the large dendrimer modifies the freezing ability of the solution toward a more glasslike behavior.

Analysis of the EPR Spectra of the Cu(II) Complexes of the Silver−Dendrimer Nanocomposites $[(Cu^{2+})_i\{(Ag^0)_m-En.A\}]$, $[(Cu^{2+})_j\{(Ag^0)_m-En.P\}]$, and $[(Cu^{2+})_k\{(Ag^0)_m-En.T\}]$. The silver ions were transformed into metal atoms by X-ray irradiation of the samples. This simple modification changed the interaction of Cu(II) with the dendrimers in the direction of favoring the internalization of copper in the dendrimer structure.

The EPR spectra were analyzed with the same computation procedure described in the previous section.

First, we examine the EPR spectra of the amino-surface-terminated dendrimer nanocomposites. Parts a−c of Figure 7 show the EPR spectra of the copper(II) ions complexed in the silver nanocomposites of various generations of amine-terminated dendrimers at the same concentration as in the previous part and at three temperatures: 358 (Figure 7a), 298 (Figure 7b), and 160 K (Figure 7c). With respect to the complex copper spectra of Ag^+−dendrimer complexes, the spectra of Ag^0−dendrimer nanocomposite complexes show interesting differences also at 358 K. The analysis of the spectra in Figures 7a−c indicates the following point:

Cu(II) mainly localizes in the interior of the dendrimer nanocomposite structure and only a small fraction of copper coordinates to dendrimer sites in the vicinity of the PAMAM surface. The coordination changes as a function of temperature and generation.

(a) At room temperature, the spectra show slow motion conditions due to the entrapment of Cu(II) in the internal dendrimer structure. The slow motion is mainly confirmed by the partial resolution of the anisotropic components at low field ($A_{||}$).

(b) Because of the fact that slow motion conditions are still retained at a temperature as high as 358 K; we expect that the partial *occupancy of the dendrimer interior by Ag^0 decreases the freedom of mobility of both the Cu(II) ions and the dendrimer branches.* Indeed, only fast motion conditions were found at high temperature in previous studies about the complexes formed between Cu(II) and PAMAM dendrimers in the absence of Ag^0.[19,20]

(c) The mobility in templates both at room and high temperatures decreased with the increase in generation, as already found in previous studies of Cu(II)−PAMAM dendrimer complexes.[19,20] In fact, smaller dendrimers have an open structure: the distances between nitrogen ligands are large and the branches have a large freedom of motion.

(d) An interesting feature is the presence of two superimposing signals in the spectra at 358 K of the small generation DNC complexes, $[(Cu^{2+})_n\{(Ag^0)_{3.77}-E2.A\}]$ and $[(Cu^{2+})_n\{(Ag^0)_{7.66}-E3.A\}]$. One signal is constituted by the four resolved hyperfine lines from which the isotropic coupling constant $\langle A \rangle$ is evaluated as about 75 G. The presence of the second signal is evidenced by the shoulder of the fourth line at high field. Probably these two signals are already present for the lowest generations at 298 K, since the fourth line is particularly broad. Since the spectrum at low temperature is constituted by a single component, we may exclude that the two superimposed signals are due to Cu(II) in two different coordination. More probably, the

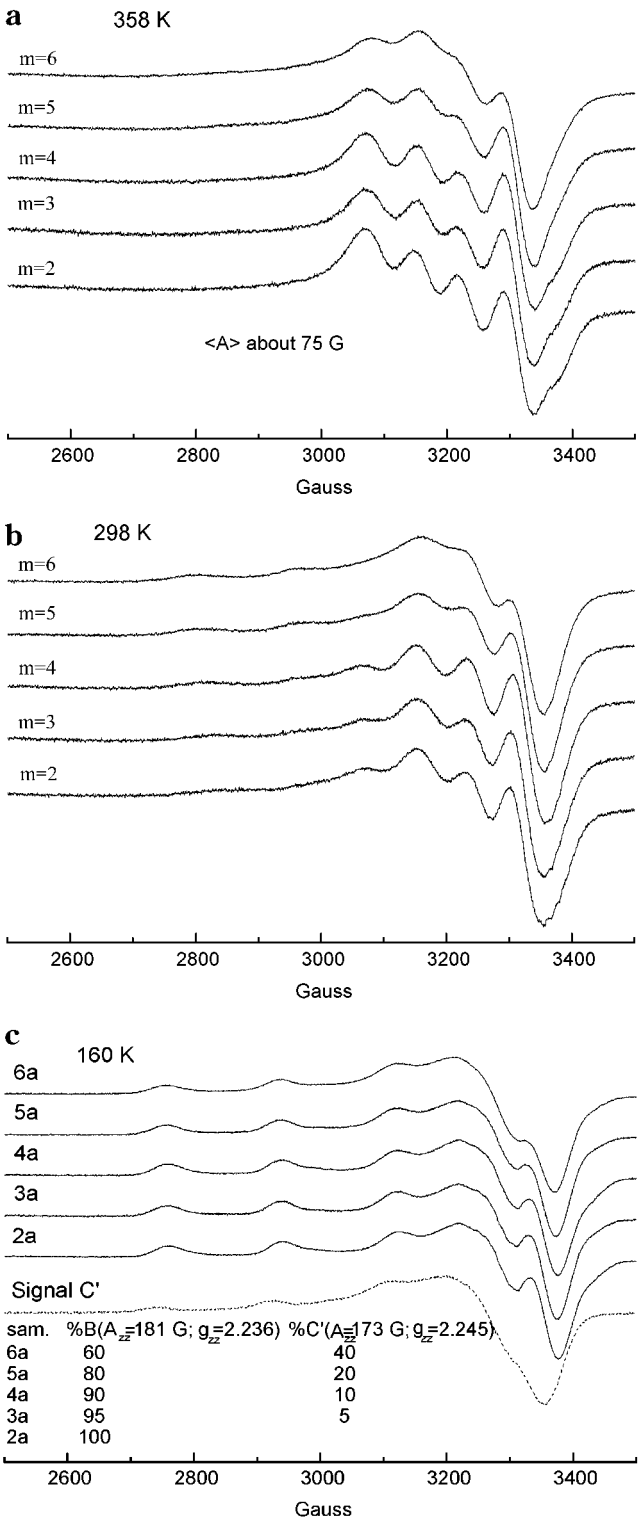

Figure 7. EPR experimental spectra (full lines) of from $[(Cu^{2+})_k\{(Ag^0)_l-Em.A\}]$ nanocomposite complexes at 358 (a), 298 (b), and160 K (c). The dashed line in part c is signal C′ extracted from the addition-subtraction procedure. For the sake of simplicity, individual spectra belonging to different complexes have been annotated by using the shorthand of their dendrimer component, i.e., "6a" refers to the copper complex of the silver nanocomposite formed with the generation 6 amine-terminated PAMAM, etc. Computation of the spectra (not shown) provides the percentages of signals B and C′ for each complex also reported in Figure 7c.

two signals arise *from almost the same copper complexes but in two different mobility conditions.* Since in the absence of silver only one signal (the four resolved lines due to fast moving copper complexes) is present inside the dendrimer,[19,20] we suggest that the second signal, due to copper complexes still slow moving at 358 K, is due to *copper complexes entrapped in the same dendrimer internal cavities as silver atoms*, which diminishes the freedom of the Cu(II) complex. This second signal gradually disappears with the increase in generation since the overall size of internal cavities in the dendrimer decrease in size and do not allow the entrance of both copper and silver. Therefore, in the cavities occupied by copper, the mobility of the complex is low at high generation even at 358 K.

(e) The analyses of the spectra (subtraction of the signal 2 from the signal of higher generations) indicate the presence of a further component, termed signal C′ (also present at room temperature), which increases in intensity at the expenses of signal B with the increase in generation. The variation in percentages of signal B and signal C′ is reported at the bottom of Figure 7c. Signal C′, reported as a dashed line in Figure 7c, *does not* correspond to signal C described for the Ag^+−dendrimer complexes: its magnetic parameters (the parallel components of the **A** and **g** tensors are also reported in the figure) are much closer to those of signal B than those of signal C. The parameters of *signal C′ correspond to copper complexes* quite similar to those responsible of signal B, that is, *Cu−N_3 or Cu−N_4, but the nitrogen centers are observed at a greater distance from copper* and at least one methanol molecule will compete with the nitrogen group for coordination with copper.

This behavior at high generation is positively due to the occupancy of the narrower cavities of the dendrimer interior by Ag^0. As a consequence, a portion of the copper is forced to occupy the larger cavities (which are closer to the core) forming less stable complexes with nitrogen centers being a longer distance from copper ions but still quenched in mobility at high temperatures.

The spectra obtained from the pivalate-terminated $[(Cu^{2+})_n\{(Ag^0)_{3.71}-E3.P\}]$ and $[(Cu^{2+})_n\{(Ag^0)_{15.87}-E5.P\}]$ are reported in Figure 8a at the three temperatures of 160, 298, and 358 K.

The spectra at 160 K are quite similar to each other indicating the presence of a variable amount of signal C, between 40 and 45%, with slightly changing line widths (about 23−25 G). The presence of such an amount of signal C is mainly unexpected for $[(Cu^{2+})_n\{(Ag^0)_{3.71}-PAMAM\_E3.P\}]$ if compared to the results from Figure 7. This means that the pivalate groups at the surface modify the behavior of the dendrimers, rendering the low generation dendrimer similar to the high generation dendrimer in its coordination ability. Consequently, the distribution of both Ag^0 and Cu^{2+} in the periphery also changes. This is confirmed by the analysis of the spectra at room and high temperature: even at 358 K, copper ions complexed by $\{(Ag^0)_{3.71}-PAMAM\_E3.P\}$ show very slow motion.

We believe that the bulky pivalate groups at the surface confer more rigidity to the dendrimer branches. As a consequence, the copper ions interact with the nitrogen ligands in more rigid dendrimer branches with Ag^0 partly impeding the close approach to the nitrogen centers.

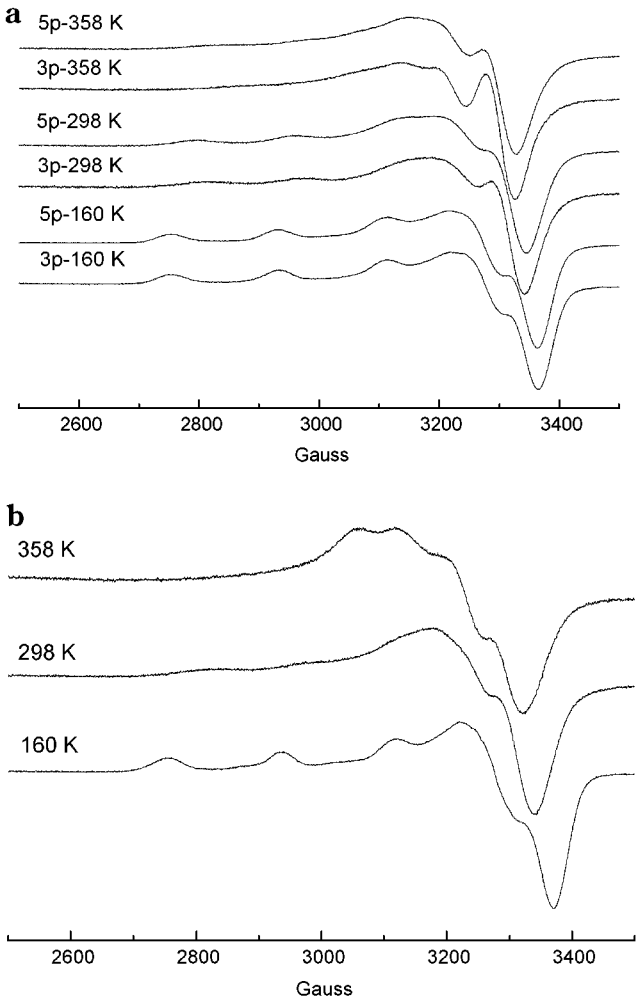

Figure 8. EPR experimental spectra (full lines), at 160, 298, and 358 K, obtained from (a) $([(Cu^{2+})_n\{(Ag^0)_{15.87}-E5.P\}]$ and $[(Cu^{2+})_n\{(Ag^0)_{3.71}-E3.P\}]$, the Cu^{2+} complexes of the nanocomposites formed from pivalate-terminated dendrimers (5p and 3p, respectively), and (b) $[(Cu^{2+})_n\{(Ag^0)_{7.41}-E4.T\}]$, the Cu^{2+} complex of a silver nanocomposite of the Tris-terminated dendrimer template.

A different situation is found for Cu(II) complex of the Tris-terminated nanocomposite $[(Cu^{2+})_n\{(Ag^0)_{7.41}-E4.T\}]$, for which spectra are shown in Figure 8b for 160, 298, and 358 K. The spectrum of E4.T is constituted by one component, termed signal B", which differs from signal B for a small decrease of the $A_{||}$ component (from 183 to 178 G). The spectrum at high temperature provides a proof of the presence of a single component with a smaller $\langle A \rangle$ (the isotropic coupling constant measured from this spectrum is about 68 G, with respect to about 75 G measured for $[(Cu^{2+})_n\{(Ag^0)_{3.71}-E3.P\}]$).

Therefore, the $\{(Ag^0)_{7.41}-E4.T\}$ nanocomposite provides homogeneous types of sites for copper complexation in the dendrimer interior. These sites are similar to those of the low generation amine-terminated nanocomposites, but give rise to a different geometry of the complexes (for sure three and not four nitrogen centers are linked) and are quite close to each other.

These conclusions regarding the internal structure of silver nanocomposites are also supported by energy-filtered TEM images using unstained specimens. On the bright field image of the $\{(Ag^0)_{14.96}-PAMAM\_E4.A\}$ nanocomposite (Figure 9), only the silver content is visible. Uniform gray areas indicate uniform distribution of silver atoms in the nanocomposite particles, while

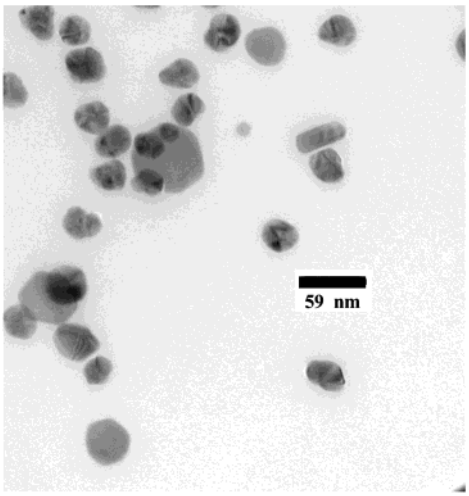

Figure 9. Bright field image of the $\{(Ag^0)_{14.96}-PAMAM\_E4.A\}$ nanocomposite. Unstained image, only the silver content is visible. Uniform gray areas are indicative of uniform distribution of the silver atoms in the hybrid nanocomposite particles.

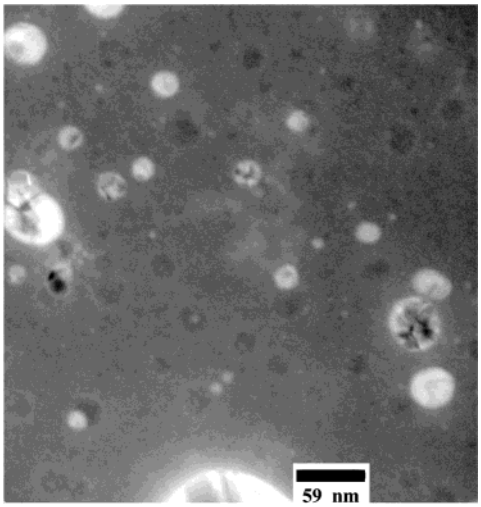

Figure 10. Dark field image of the $\{(Ag^0)_{7.41}-E4.T\}$ silver nanocomposite. Dendrimers appear as light areas while silver is represented by the fine dark lines within the polymeric matrix (unstained specimen with energy filter).

incresing density indicative of the formation of small silver metallic domains is observed toward the core. Sample preparation on a grid may lead to structural changes in the resulting particles as solvent evaporation followed by high vacuum will promote the association of nanocomposite particles. However, the procedure cannot reverse the formation of silver nanodomains and cannot lead to the formation of particles with homogeneous silver domains, unless they have existed before the sample preparation. (Silver complexes should also provide uniform gray images, but silver ions cannot exist in TEM due to the high energy electron beam.) Overlap of some of these homogeneously loaded particles can also be observed in Figure 9 indicating clustering of individual particles. How much these aggregations are the consequence of TEM sample preparation technique is unknown yet. In most of the nanoparticles, combination of gray and small black areas shows that nanosized silver(0) domains have already developed within the nanocomposite particles. This type of image also suggests that hybrid particles containing uniform distribution of metal ions in a dendrimer matrix may gradually undergo phase separation and small metallic domains develop within the polymer phase. This feature is demonstrated by the second example in Figure 10, a dark field image of the $\{(Ag^0)_{7.41}-E4.T\}$ silver nanocomposite. Here, dendrimers appear light while the fine dark lines within the polymeric matrix show the internal silver structure of the nanoparticles. We speculate, that metal atoms interact stronger within each other than with the organic matrix, a fine structure forms in time wherever silver atoms are close to each other or the matrix is locally less dense.

On the basis of these experiments and reasoning, we conclude that silver ions are distributed homogeneously in complexes, and silver metal atoms in the nanocomposites primarily occupy the narrower cavities of the dendrimer matrix and form secondary structures.

Conclusions

Silver complexes and nanocomposites of various PAMAM dendrimers were constructed at a constant silver and amine concentration ratio. First an Ag^+–dendrimer complex was obtained, and then the silver ions were transformed from Ag^+ to Ag^0 by irradiating the complex solution with an excessive dose of X-rays to avoid alteration of the structure of the complexes during transformation into nanocomposites. Because of the varying generations (from 2 to 6) and terminal groups (amine, pivalate, and Tris) of the dendrimer templates, the molecular masses and the silver/dendrimer ratios were different in each case. Intensity of the silver(0) plasmon resonance in the dendrimer nanocomposite solutions was found to be a function of nanoparticle size and architecture—lower generations resulted in peaks of lower intensity.

EPR spectra were obtained by adding Cu^{2+} solutions to the Ag^+–dendrimer complexes and to the Ag^0–dendrimer nanocomposites. Detailed computer-aided EPR analysis revealed that the internal structure of the dendrimer–silver ion complexes changed during their transformation into nanocomposites as different internal coordination were recognized for Cu^{2+} in the dendrimer network in the complexes and in the respective silver nanocomposites. In the presence of silver ions, the interior of the dendrimer is positively charged and partly repulsed copper ions, which were largely confined to sites not taken by the silver ions. The mobility of Cu(II) is quenched due to the internalization in the dendrimer structure. The Tris surface provides a stronger constraint of the dendrimer structure with respect to pivalate in the region in which the Cu–dendrimer complex forms. Relatively, a lower degree of Cu^{2+} binding occurs inside the $[(Ag^+)_m-PAMAM\_En.A]$ silver complexes of amine-terminated dendrimers, with respect to the pivalate $[(Ag^+)_m-PAMAM\_En.P]$ and $[(Ag^+)_m-PAMAM\_En.T]$ Tris-terminated ones.

Transformation of Ag^+ into Ag^0 completely modifies the Cu(II) interaction with the dendrimer in the direction of favoring the internalization of copper(II) ions in the dendrimer structure. In nanocomposites, Ag^0 atoms primarily occupied the narrow cavities of the dendrimer interior, forcing a portion of copper ions into the larger cavities. Due to the presence of Ag^0 both the freedom of mobility of the Cu(II) ions and of the dendrimer branches decreases. The mobility (both at room and high temperatures) decreases with the increase in generation.

Redistribution of the available ligands occurred in silver ion–dendrimer complexes upon addition of the copper ion probes. Formation of silver ion complexes

reduced the mobility of the copper ion probes and increased the rigidity of the dendrimer structure. When silver ions in the Ag complexes were transformed into zerovalent atoms, they lost both their charge and mobility. These silver atoms remained in the narrow cavities of the PAMAM dendrimer network and efficiently blocked them from copper ion probes. Energy-filtered TEM images have demonstrated the partial phase separation of the silver in the polymeric matrix of the nanocomposite particles.

Acknowledgment. M.F.O. thanks the Italian Ministero per la Ricerca Scientifica e Tecnologica (MURST) for the financial support. R.V. thanks Drs. Wolfgang Probst and Erhardt Zellmann of Leo Electron Microscopes in Oberkochen, Germany, and Sam Gido for access to Keck- and NSF−MRSEC-funded EM facilities at the Keck Morphology Laboratory, University of Massachusetts, Amherst, MA. L.B. expresses thanks for the partial support of DARPA under Contract MDA972-97-1-0007, titled "Nanomolecule-Based Agents for Pathogen Counter Measure." (P.I.: James R. Baker).

References and Notes

(1) Balogh, L.; Swanson, D. R.; Spindler, R.; Tomalia, D. A. *Proc. ACS PMSE* **1997**, *77*, 118.
(2) Balogh, L.; Tomalia, Donald, A. *J. Am. Chem. Soc.* **1998**, *120*, 7355.
(3) Zhao, Mingqi; Sun, Li; Crooks, R. M. *J. Am. Chem. Soc.* **1998**, *120*, 4877−4878.
(4) Sooklal, K.; Hanus, L. H.; Ploehn, H. J.; Murphy, C. J. *Adv. Mater.* **1998**, *10* (14), 1083.
(5) Esumi, K.; Suzuki, A.; Aihara, N.; Usui, K.; Torigoe, K. *Langmuir* **1998**, *14*, 3157−3159.
(6) Balogh, L.; Valluzzi, R.; Hagnauer, G. L.; Laverdure, K. S.; Gido, S. P.; Tomalia, D. A. *J. Nanoparticle Res.* **1999**, *1*, 353.
(7) Hirai, H.; Aizawa, H.; Shiozaki, H. *Chem. Lett.* **1992**, 1527.
(8) Chan, Y. Ng Cheong; Schrock, R. R.; Cohen, R. E. *J. Am. Chem. Soc.* **1992**, *114*, 7295.
(9) Saito, R.; Okamura, S.-I.; Ishizu, K. *Polymer* **1996**, *37*, 5255.
(10) Balogh, L.; Tomalia, D. A.; Hagnauer, G. L. *Chem. Innovation* **2000**, *March*, 19−26.
(11) Balogh, L.; Laverdure, K. S.; Gido, S. P.; Mott, A. G.; Miller, M. J.; Ketchel, B. P.; Tomalia, D. A. *Mater. Res. Soc. Symp. Proc.* **1999**, *576*, 69−75.
(12) Zhao, M.; Crooks, R. M. *Chem. Mater.* **1999**, *11*, 3379−3385.
(13) Rubin, S.; Bar, G.; Cutts, R. W.; Zawodzinski, T. A., Jr. *Proc. Electrochem. Soc.* **1995**, 151.
(14) Rubin, S.; Cutts, R. W.; Taylor, T. N.; Zawodzinski, T. A., Jr. *Langmuir* **1996**, *12*, 5, 1172.
(15) Grohn, F.; Bauer, B. J.; Akpalu, Y. A.; Jackson, C. L.; Amis, E. J. *Macromolecules* **2000**, *33*, 6042−6050.
(16) (a) Beck Tan, N.; Balogh, L.; Trevino, S. *Polym. Mater. Sci. Eng.* **1997**, *77*, 120. (b) Beck Tan, N.; Balogh, L.; Trevino, S.; Tomalia, D. A.; Lin, J. S. *Hybrid Mater., Mater. Res. Soc. Symp. Proc.* **1998**, *519*, 143−150. (c) Beck Tan, N.; Balogh, L.; Trevino, S.; Tomalia, D. A.; Lin, J. S. *Polymer* **1999**, *40*, 2537−2545.
(17) Martell, A. E.; Hancock, R. D. In *Modern Inorganic Chemistry*; Prackler, J. P., Jr., Ed.; Plenum Press: New York, 1996.
(18) Diallo, M.; Balogh, L.; Shafagati, A.; Johnson, J. H., Jr.; Goddard, W. A., III; Tomalia, D. A. *Environ. Sci. Technol.* **1999**, *33*, 820−824.
(19) Ottaviani, M. F.; Bossmann, S.; Turro, N. J.; Tomalia, D. A. *J. Am. Chem. Soc.* **1994**, *116*, 661−671.
(20) Ottaviani, M. F.; Montalti, F.; Turro, N. J.; Tomalia, D. A. *J. Phys. Chem. B* **1997**, *101*, 2, 158−166.
(21) *Lange's Handbook of Chemistry*, 15th ed.; Dean, J. A., Ed.; McGraw-Hill: New York, 1999; pp 883.
(22) Balogh, L.; Fry, J.; Orszagh, I. Manuscript in preparation.
(23) Venkataraman, D.; Lee, S.; Moore, J. S.; Zhang, P.; Hirsch, K. A.; Gardner, G. B.; Covey, A. C.; Prentice, Ch. L.; *Chem. Mater.* **1996**, *8*, 2030−2040.
(24) Schneider, D. J.; Freed, J. H. In *Spin Labeling: Theory and Applications*; *Vol. III, Biological Magnetic Resonance*; Berliner, L. J., Reuben, J., Eds.; Plenum Press: New York, 1989; Vol. 8, p 1.
(25) Doremus, R. H.; Rao, P. *J. Mater. Res.* **1996**, *11*, 2834.
(26) Because of the complex structure, we use the following convention to describe the composition of the synthesized nanomaterials: brackets denote complexes as is common while braces represent nanocomposite structures. Within the brackets or braces, first the complexed/encapsulated components are listed (with an index of their average number per dendrimer molecule) and then the family of dendrimers followed by terms used for dendrimer identification, i.e., core, generation, and surface. For example a three-component composite is described by the following general formula: {(comp #1)$_i$ (comp #2)$_j$ (comp #3)$_k$ − DENDRIMER_CoreGeneration.Terminal group}. Thus, the formula of {$(Ag^0)_{14}$−PAMAM_E4.A} denotes a silver dendrimer nanocomposite in which a generation four amine-terminated ethylenediamine (EDA or E for short) core poly(amidoamine) (PAMAM) dendrimer contains 14 zerovalent silver atoms. Accordingly, [$(Cu^{2+})_5${$(Ag^0)_{3.77}$−PAMAM_E3.P}] denotes the copper complex of a silver nanocomposite containing five copper ions and 3.77 silver atoms per dendrimer on average and the dendrimer used is an EDA core generation three PAMAM dendrimer with 16 pivalate groups as termini. Similarly, [$(Cu^{2+})_7(Ag^+)_7$−PAMAM_E4.T] denotes the copper complex of an EDA core generation four Tris surface PAMAM containing seven cupric ions and seven silver ions per dendrimer. The above scheme provides a relatively simple but consistent way to identify materials with a complicated structure. In this paper, as only PAMAM dendrimers were used, we usually followed the shorter pattern and omitted naming the dendrimer. This way, [$Cu^{2+})_5${$(Ag^0)_{3.77}$−PAMAM_E3.P}] and [$(Cu^{2+})_5${$(Ag^0)_{3.77}$−E3.P}] are considered to be equivalent names.]

MA010492F